

See discussions, stats, and author profiles for this publication at: <https://www.researchgate.net/publication/234800181>

Ray Tracing Volume Densities

Article in ACM SIGGRAPH Computer Graphics · July 1984

DOI: 10.1145/964965.808594

CITATIONS

660

READS

2,970

2 authors, including:



[Brian von Herzen](#)

Rapid Prototypes, Inc.

21 PUBLICATIONS 1,430 CITATIONS

SEE PROFILE

RAY TRACING VOLUME DENSITIES

James T. Kajiya
Brian P. Von Herzen

California Institute of Technology
Pasadena, Calif

ABSTRACT This paper presents new algorithms to trace objects represented by densities within a volume grid, e.g. clouds, fog, flames, dust, particle systems. We develop the light scattering equations, discuss previous methods of solution, and present a new approximate solution to the full three-dimensional radiative scattering problem suitable for use in computer graphics. Additionally we review dynamical models for clouds used to make an animated movie.

KEYWORDS: computer graphics, raster graphics, ray tracing, stochastic modelling, simulation of natural phenomena, radiative transport, light scattering, clouds, particle systems.

CR CATEGORIES: I.3.3, I.3.5, I.3.7

§1 Introduction

A large class of natural phenomena is described by partial differential equations. In almost all cases, the description of these phenomena is given by a set of vector or scalar fields defined on a uniform mesh in 3-space. This paper will render objects defined in this way via the ray tracing method (Whitted 1980, Appel 1968, Goldstein 1971, Kajiya 1982, 1983).

Recently, the synthesis of images with clouds and, more generally, of objects defined as volume densities has been pursued by a number of investigators (Blinn 1982, Max 1983, Voss 1983). This paper is a continuation of that work in the context of ray tracing.

Blinn introduced the use of density models in computer graphics in Blinn (1982), where he considers plane parallel atmospheres. Other researchers have adapted

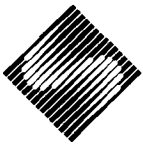
his models to more general shapes. Max defines clouds as densities with boundaries defined by analytic functions. Voss has fractally generated densities with a series of plane parallel models, yielding images of striking realism.

The work presented here extends previous efforts in two ways: first, we present an alternative to the Blinn scattering model which models multiple radiative scattering against particles with high albedo. Second, we show how to ray trace these models.

We emphasize that the rendering techniques presented here are general. We are able to view the models from any angle, with multiple arbitrarily placed light sources (even within the densities). The density model may intersect other procedural models. The viewing point may lie inside the density function. With these techniques we are able to render clouds that cast shadows on their environment as well as on themselves. We may have scenes in which mountain peaks disappear into a cloud interior. We may fly through the clouds. And, of course, the clouds appear reflected and refracted in other objects in the scene. There is one situation, however, which we do not handle correctly: other procedural objects, while they may be shadowed accurately by clouds, do not themselves cast shadows upon the clouds.

While clouds are the most obvious application of this representation, other phenomena also lend themselves well to this representation. For example, it is possible to model media which do not simply scatter, but also absorb and emit light. In this way we can model flames. Additionally, it is possible to generate models of very high geometric complexity which are treated simply as volume densities. In this way these techniques allow the application of ray tracing to Reeves' particle systems (Reeves 1983).

Permission to copy without fee all or part of this material is granted provided that the copies are not made or distributed for direct commercial advantage, the ACM copyright notice and the title of the publication and its date appear, and notice is given that copying is by permission of the Association for Computing Machinery. To copy otherwise, or to republish, requires a fee and/or specific permission.



§2 The scattering equation

In this section we discuss the relevant physical parameters and set up an equation which describes the scattering of radiation in volume densities. This section loosely follows the derivation in Chandrasekhar (1950).

The quantity to be calculated in a scattering problem is the energy per unit solid angle per unit area:

$$dE = I(x, \omega) \sin \vartheta d\omega d\sigma$$

This quantity is called the *intensity* of radiation at a point x in the direction of the solid angle $d\omega$.

The scattering equation can be derived by considering a differential cylindrical volume $dV = d\sigma ds$, where $d\sigma$ is the cross section of the cylinder and ds is the length (figure 1). If we follow a pencil of radiation along the length of the cylinder, we find that the difference in intensity between the two ends is given by

$$\begin{aligned} dI &= -\text{absorbed} + \text{emitted} \\ &= -\kappa \rho ds d\sigma d\omega + j \rho ds d\sigma d\omega \end{aligned} \quad (2.1)$$

where ρ is the density of matter in the volume element; κ is the absorption coefficient, viz. optical depth per unit density; and j is the emission coefficient.

The emission coefficient can be broken into two terms

$$j = j^{(e)} + j^{(s)}$$

where $j^{(e)}$ is the emission coefficient due to pure emission of the medium, for example a black body term for flames or stellar interiors; and $j^{(s)}$ is the emission term due to pure scattering of incident radiation into the direction of interest. The form of this term is usually written as

$$j^{(s)} = \kappa \frac{1}{4\pi} \int_{\|\bar{s}\|=1} p(s, \bar{s}) I(x, \bar{s}) d\bar{s}.$$

This expression says that the light scattered in direction s is a linear operator of the light incident upon the volume element from all angles. The function $p(s, \bar{s})$ is called the *phase function* and gives the amount of light scattered from direction s to direction \bar{s} . In many situations the medium is *isotropic*, in the case the phase function depends only on the *phase angle* Θ , the angle between s and \bar{s} . Although there are many interesting phenomena in which the emission coefficient $j^{(e)}$ is nonzero, let us for simplicity assume it is zero in the remainder of this paper.

The phase function embodies all the information about the scattering behavior of the medium. From it we may

derive all the other lighting parameters popular in computer graphics. For example, Lambert and Phong surfaces are simply phase functions with particular shape parameters. In these cases anisotropy prevails: there are preferred angles—for example, the normal of the surface element. Thus the phase function varies with more than just the phase angle. When the medium is composed of a large number of particles, no preferred orientations occur and isotropy obtains. In this case the phase angle completely determines the phase function value. Blinn (1982) discusses a number of important phase functions. For the work on clouds, two will be of particular interest: 1) perfectly diffuse scattering: $p(\cos \Theta) = \varpi_0$ where ϖ_0 is an arbitrary constant, and 2) Rayleigh scattering: $p(\cos \Theta) = \varpi_0 \frac{3}{4} (1 + \cos^2 \Theta)$.

The scattering equation can be brought into general form by dividing both sides of equation (2.1) by $-\kappa \rho ds$. But the derivative along the cylinder is simply a directional derivative along s

$$\frac{dI}{ds} = s \cdot \nabla_x I.$$

This gives us the scattering equation:

$$\begin{aligned} -\frac{1}{\kappa \rho} s \cdot \nabla_x I(x, s) - I(x, s) \\ + \frac{1}{4\pi} \int_{\|\bar{s}\|=1} p(s, \bar{s}) I(x, \bar{s}) d\bar{s} = 0. \end{aligned}$$

§3 Solving the scattering equation

The scattering equation is solvable analytically only in a few very special cases: indeed, it is very difficult to solve even numerically without assumptions which reduce the dimensionality of the intensity field $I(x, s)$, a function of six real variables.

Various assumptions are customarily made to reduce the difficulty of the problem. Here are some common assumptions: 1) the medium is *isotropic*—the phase function is only dependent on the phase angle; 2) the medium is uniform—its density does not change from point to point in space; 3) the geometry is simple—the medium may vary in space but only along, say, the z -axis (this is the *plane parallel* or scattering in a slab problem); 4) the phase function is of a very simple type, viz. isotropic; 5) the albedo is very small or very large.

Various combinations of these assumptions have been treated extensively in the literature. The slab scattering problem has been the most common assumption (Chandrasekhar 1950).

The method of Wick-Chandrasekhar or *discrete ordinates* is a numerical method for plane parallel atmospheres. It sets up a coupled array of PDEs each of which represents one scattering angle. A finite Euler approximation is made for the phase integral which is the coupling mechanism of the individual equations. Convergence results for such approximations have appeared in Keller (1960ab) and more recently Anselone and Gibbs (1974).

Unfortunately, the discrete ordinates method is relatively unsuitable for computer graphics: we need to most often finely sample a given portion of the solid angle sphere, rather than have a uniform sampling across the whole sphere.

It may well be that a finite element approach would be a promising alternative to Wick-Chandrasekhar, but we have found that simpler schemes are effective for image synthesis.

3.1 Blinn's Low Albedo approximation

Blinn (1982) was the first to introduce a volume density scattering model to computer graphics. In this paper he made a number of approximations well suited to the problem he was studying: the rings of Saturn. Blinn chose to model a uniform medium of relatively low albedo with a single illuminating light source. (Although his method generalizes easily to multiple light sources.)

Assuming the above and, in addition, only a *single scattering* of the radiation from the light source to the eye, he was able to solve the problem analytically. Of course, multiple scattering is a second order effect for a medium with low albedo. The Blinn model is thus valid for a wide variety of phenomena.

Voss (1983) has adapted Blinn's procedure to more general geometries, by essentially modelling a sandwich of several Blinn models. With it, he has made some exceptional images of clouds. Both the Blinn and Voss methods place restrictions on the lighting and viewing geometry of the scene.

Unfortunately, clouds have a very high albedo—the single scattering approximation does not hold. A number of visible defects appear when rendering by the new technique. This is because the older method imposed viewing geometry restrictions which hid the defects.

It is one finding of this paper that realistic rendering of clouds demands more accuracy in the scattering model.

3.2 A ray tracing algorithm for the low albedo case

In this section we will describe a new technique which

allows one to ray trace volume densities without any viewing or lighting restrictions. But for one slight twist, this method is essentially a brute force development of the Blinn single scattering model for ray tracing.

The key to the new method is that it separates the rendering procedure into two steps. The first step drives the radiation from light source i through a density array $\rho(x, y, z)$ into an array $I_i(x, y, z)$ which holds the contribution of each light source to the brightness of each point in space. This is done simply by calculating in parallel the following line integrals for each path $\Gamma_{x,y,z} = (x(t), y(t), z(t))$ from the light source through $\rho(x, y, z)$.

$$I_i(x, y, z) = \exp\left(-\tau \int_{\Gamma_{x,y,z}} \rho(\gamma) d\gamma\right)$$

where $\kappa = \tau\rho$. The principal observation is that this computation need only be done from at most once per frame to at least once per scene.

The second step occurs once per ray trace. Each ray is first culled against a bounding rectangular prism as an extent. The brightness of a ray sums the contribution of each volume element. It is given by:

$$B = \int_{\lambda_1}^{\lambda_2} e^{-\tau \int_{\lambda_1}^t \rho(x(\mu), y(\mu), z(\mu)) d\mu} \times \left[\sum_i I_i(x(t), y(t), z(t)) p(\cos \Theta_i) \right] \times \rho(x(t), y(t), z(t)) dt$$

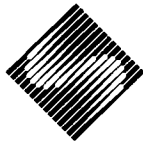
In this expression, λ_1, λ_2 are the beginning and ending of the path between the eye and furthest visible volume element. It is set by

$$\lambda_1 = \max(0, d_1) \\ \lambda_2 = \min(d_{\text{global}}, d_2)$$

Where d_1 is the distance to the nearest intersection point with the bounding extent, d_{global} is the distance to the nearest intersection point with the rest of the world database, and d_2 is the distance to the farthest intersection point with the bounding extent.

The first exponential in the brightness integral gives the amount of attenuation due to absorption and scattering of the material visible to the eye. The sum term gives the brightness contribution of each light source to the brightness of the particular point.

According to the integral there are two remaining steps which must be done. The first is to compute the integrated optical path length along a particular ray.



This is done by simply bilinearly sampling and summing the density array along the ray. The second step is to compute and sum the actual brightness integral. Note that each of the integral terms has been precomputed so that a point sampling is all that is needed to compute the brightness term. We have used the Romberg integration method to actually compute the integral (Dahlquist and Bjork 1974).

§4 High Albedo approximation.

The low albedo approximation suffers from a number of defects when used to model clouds, a scattering medium of very high albedo. This can be seen in the results section. There are portions of the clouds which are abnormally dark due to shadowing of one part of a cloud upon another. In the actual physical situation these dark portions are illuminated by the second and higher order scattering centers within the cloud.

If one observes these clouds from above, the shadowing problem is not observable, since the eye and the light source are on the same side of the cloud. When looking from the underside of the cloud on the opposite side of the light source, one cannot determine what the actual thickness of the cloud is, so again the eye cannot discern an artificial darkening. However, clouds observed to shadow themselves viewed from the side show this problem quite clearly (see the figures).

Blinn (1982) has suggested treating the multiple scattering problem by a Neumann expansion involving the phase integral. This method is likely to work well only with lower albedo media, since the series is geometric in the albedo ω_0 . If the albedo ω_0 is close to one, many terms will be needed to converge to a solution.

4.1 A Perturbation solution, conservative systems

In order to approximate the high albedo solution, we perform a perturbation expansion on $\beta = (1 - \omega_0)$. We normalize the phase function to

$$\begin{aligned} p(\Theta) &= \omega_0 \bar{p}(\Theta) \\ &= (1 - \beta) \bar{p}(\Theta) \end{aligned}$$

For compactness, we write the scattering equation

$$\begin{aligned} &-\frac{1}{\kappa\rho} s \cdot \nabla_x I(x, s) - I(x, s) \\ &+ \frac{1}{4\pi} (1 - \beta) \int_{\|\bar{s}\|=1} \bar{p}(s, \bar{s}) I(x, \bar{s}) d\bar{s} = 0 \end{aligned}$$

as the sum of two linear operators

$$LI + (1 - \beta)MI = 0$$

where

$$\begin{aligned} LI &= -\frac{1}{\kappa\rho} s \cdot \nabla_x I(x, s) - I(x, s) \\ MI &= \frac{1}{4\pi} \int_{\|\bar{s}\|=1} \bar{p}(s, \bar{s}) I(x, \bar{s}) d\bar{s}. \end{aligned}$$

Expanding I into a power series in β gives

$$I = \sum_{k=0}^{\infty} \beta^k I_k.$$

Substituting into the original equation for I and equating like powers of β gives a set of equations

$$LI_k + MI_k = -MI_{k-1}.$$

Thus the perturbation solution presents us with a series of forced conservative ($\omega_0 = 1$) scattering equations. We now develop techniques which allow us to approximate the solutions for the conservative case.

4.2 The Scattering equation expressed in Spherical Harmonics

We expand $I(x, s)$ into spherical harmonics in s to obtain

$$I(x, s) = \sum_{l=0}^{\infty} \sum_{m=-l}^l I^{lm}(x) Y_{lm}(s).$$

The functions Y_{lm} are the customary normalized spherical harmonics of degree l and order m

$$Y_{lm}(\vartheta, \phi) = P_{lm}(\vartheta, \phi) e^{im\phi}$$

where the P_{lm} are the associated Legendre polynomials of degree l and order m (Courant and Hilbert 1953).

Substituting the spherical harmonic expansion into the scattering equation we obtain

$$\begin{aligned} &\sum_{l,m} -\frac{1}{\kappa\rho} s \cdot [\nabla I^{lm}(x)] Y^{lm}(s) - I^{lm}(x) Y_{lm}(s) \\ &+ I^{lm} \int p(s, \bar{s}) Y_{lm}(\bar{s}) d\bar{s} = 0. \end{aligned}$$

Multiplying this equation by $Y_{l'm'}^*(s)$ and integrating we get

$$\sum_{l,m} \frac{1}{\kappa\rho} \nabla I^{lm}(x) \cdot \int Y_{l'm'}^*(s) s Y_{lm}(s) ds - I^{lm}(x) \delta_{ll'} \delta_{mm'} + \int \int Y_{l'm'}^*(s) p(s \cdot \bar{s}) Y_{lm}(\bar{s}) d\bar{s} ds = 0$$

or, writing it in Dirac "bra-ket" notation

$$\sum_{l,m} \frac{1}{\kappa\rho} \nabla I^{lm}(x) \cdot \langle Y_{l'm'}(s) | s | Y_{lm}(s) \rangle - I^{lm}(x) \delta_{ll'} \delta_{mm'} + I^{lm}(x) \langle Y_{l'm'}(s) | p | Y_{lm}(s) \rangle = 0;$$

where we write $\langle X | O | Y \rangle$ for the integral

$$\int_0^\pi \int_{-\pi}^\pi X^* O Y \sin \vartheta d\phi d\vartheta.$$

This gives us a coupled set of first order PDEs for $I^{lm}(r)$. If we know the coupling coefficients given by the matrix elements

$$\langle Y_{l'm'}(s) | p | Y_{lm}(s) \rangle$$

and

$$\langle Y_{l'm'}(s) | s | Y_{lm}(s) \rangle$$

then we can solve this system by relaxation. For graphics applications, only the first few spherical harmonics are necessary for a convincing image. We truncate the so-called "p-wave", viz. after the $l = 1$ term. The next order of business is then to calculate the matrix coupling coefficients.

4.3 Matrix elements for the position

To calculate the matrix element $\langle Y_{l'm'}(s) | s | Y_{lm}(s) \rangle$ for the direction operator s , we calculate the matrix element for each component of s ,

$$\begin{aligned} \langle Y_{l'm'}(s) | x | Y_{lm}(s) \rangle &= \langle Y_{l'm'}(s) | \sin \vartheta \cos \phi | Y_{lm}(s) \rangle \\ \langle Y_{l'm'}(s) | y | Y_{lm}(s) \rangle &= \langle Y_{l'm'}(s) | \sin \vartheta \sin \phi | Y_{lm}(s) \rangle \\ \langle Y_{l'm'}(s) | z | Y_{lm}(s) \rangle &= \langle Y_{l'm'}(s) | \cos \vartheta | Y_{lm}(s) \rangle. \end{aligned}$$

Now we may save a bit of work by setting

$$\begin{aligned} u &= x + iy \\ &= \sin \vartheta e^{i\phi}. \end{aligned}$$

Now,

$$\begin{aligned} \langle Y_{l'm'}(s) | u | Y_{lm}(s) \rangle &= \int [P_{lm}(\cos \vartheta) e^{im\phi}]^* [P_{l'm'}(\cos \vartheta) e^{im'\phi}] \\ &\quad \times e^{i\phi} \sin^2 \phi d\vartheta d\phi \\ &= \left[\int_0^\pi P_{lm}(\cos \vartheta) P_{l'm'}(\cos \vartheta) \sin^2 \vartheta d\vartheta \right] \\ &\quad \times \left[\int_{-\pi}^\pi e^{i(m-m'+1)\phi} d\phi \right] \\ &= \left[\int_0^\pi P_{lm}(\cos \vartheta) P_{l'm'}(\cos \vartheta) \sin^2 \vartheta d\vartheta \right] \delta_{m+1,m'} 2\pi. \end{aligned}$$

Letting $\mu = \cos \vartheta$ and taking into account the Kronecker δ , the matrix element becomes:

$$\langle Y_{l'm'}(s) | u | Y_{lm}(s) \rangle = \int_{-1}^1 P_{lm}(\mu) P_{l'm+1}(\mu) (1-\mu^2)^{1/2} d\mu \quad (4.1)$$

But from a recursion relation for the Legendre polynomial we have

$$P_{l,m+1}(\mu)(1-\mu^2)^{1/2} = k_0 P_{l+1,m} - k_1 P_{l-1,m},$$

where

$$\begin{aligned} k_0 &= \frac{(l-m+1)(l-m+2)}{2l+1} \\ k_1 &= \frac{(l+m-1)(l+m)}{2l+1}. \end{aligned}$$

Using this relation in equation (4.1) we obtain

$$\begin{aligned} \langle Y_{l'm'}(s) | u | Y_{lm}(s) \rangle &= \int_{-1}^1 P_{l'm}(\mu) [k_0 P_{l+1,m}(\mu) - k_1 P_{l-1,m}(\mu)] d\mu \\ &= k_0 \delta_{l',l+1} - k_1 \delta_{l',l-1}. \end{aligned}$$

The last equality follows from the orthogonality for the Legendre polynomials. Since

$$\begin{aligned} x &= \text{Re}(u) \\ y &= \text{Im}(u) \end{aligned}$$

we have

$$\begin{aligned} \langle Y_{l'm'}(s) | x | Y_{lm}(s) \rangle &= \langle Y_{l'm'}(s) | u | Y_{lm}(s) \rangle \\ \langle Y_{l'm'}(s) | y | Y_{lm}(s) \rangle &= 0. \end{aligned}$$



Now to compute the z matrix element we get

$$\begin{aligned}
 \langle Y_{l'm'}(s) | z | Y_{lm}(s) \rangle &= \left[\int_0^\pi P_{l'm'}(\cos\vartheta) P_{lm}(\cos\vartheta) \cos\vartheta \sin\vartheta d\vartheta \right] \\
 &\quad \times \left[\int_{-\pi}^\pi e^{i(m-m')\phi} d\phi \right] \\
 &= \left[\int_0^\pi P_{l'm'}(\cos\vartheta) P_{lm}(\cos\vartheta) \cos\vartheta \sin\vartheta d\vartheta \right] \delta_{mm'} 2\pi \\
 &= \left[\int_{-1}^1 P_{l'm'}(\mu) P_{lm}(\mu) \mu d\mu \right] \delta_{mm'} 2\pi. \quad (4.2)
 \end{aligned}$$

Now from a recursion relation for the Legendre polynomial P_{lm} we have

$$\mu P_{lm}(\mu) = k_2 P_{l+1,m}(\mu) - k_3 P_{l-1,m}(\mu)$$

where

$$\begin{aligned}
 k_2 &= \frac{l+m}{2l+1} \\
 k_3 &= \frac{l-m+1}{2l+1}.
 \end{aligned}$$

Substituting into (4.2) we obtain

$$\begin{aligned}
 \langle Y_{l'm'}(s) | z | Y_{lm}(s) \rangle &= \int_{-1}^1 P_{l'm'}(\mu) [k_2 P_{l+1,m}(\mu) - k_3 P_{l-1,m}(\mu)] d\mu \\
 &= [k_2 \delta_{l',l+1} - k_3 \delta_{l',l-1}] \delta_{mm'} 2\pi,
 \end{aligned}$$

where the last equality follows from the orthogonality of the P_{lm} .

4.4 Matrix elements for the phase integral

We assume the phase function to vary with the phase angle only. In this case we may expand the phase function into Legendre polynomials

$$p(\cos\Theta) = \sum_{k=0}^{\infty} \varpi_k P_k(\cos\Theta)$$

and substitute into the matrix expression

$$\begin{aligned}
 \langle Y_{l'm'}(s) | p | Y_{lm}(s) \rangle &= \int_{\|s\|=1} \int_{\|\bar{s}\|=1} Y_{l'm'}^*(\bar{s}) \left[\sum_k \varpi_k P_k(s \cdot \bar{s}) \right] \\
 &\quad \times Y_{lm}(s) d\bar{s} ds \\
 &= \sum_k \varpi_k \int \int Y_{l'm'}^*(\bar{s}) P_k(s \cdot \bar{s}) Y_{lm}(s) d\bar{s} ds. \quad (4.3)
 \end{aligned}$$

Now, $s \cdot \bar{s}$ in polar coordinates is

$$\begin{aligned}
 s \cdot \bar{s} &= \cos\gamma \\
 &= \cos\vartheta \cos\bar{\vartheta} + \sin\vartheta \sin\bar{\vartheta} \cos(\phi - \bar{\phi}).
 \end{aligned}$$

This allows us to apply Laplace's formula,

$$P_l(\cos\gamma) = \frac{4\pi}{2l+1} \sum_{m=-l}^l Y_{lm}(\vartheta, \phi) Y_{lm}^*(\bar{\vartheta}, \bar{\phi}).$$

Using this identity in (4.3) we obtain

$$\begin{aligned}
 \langle Y_{l'm'}(s) | p | Y_{lm}(s) \rangle &= \sum_k \varpi_k \frac{4\pi}{2k+1} \\
 &\quad \times \sum_{p=-k}^k \left[\int Y_{l'm'}(\bar{s}) Y_{kp}^*(\bar{s}) d\bar{s} \right] \left[\int Y_{lm}^*(s) Y_{kp}(s) ds \right] \\
 &= \sum_k \varpi_k \frac{4\pi}{2k+1} \sum_{p=-k}^k \delta_{l'k} \delta_{m'p} \delta_{lk} \delta_{mp} \\
 &= \sum_k \varpi_k \frac{4\pi}{2k+1} \delta_{l'k} \delta_{lk} \delta_{m'm} \\
 &= \frac{4\pi}{2l+1} \varpi_l \delta_{l'l} \delta_{m'm}.
 \end{aligned}$$

So the phase function matrix is diagonal with respect to spherical harmonics: no scattering occurs between different spherical harmonics. Each diagonal element is given by the Legendre expansion coefficients ϖ_k .

§5 Generating density models

There are many ways to generate volume density models for the above procedure. Voss (1983) has used fractal densities with great success. We show a number of images based on these. In our images we follow Voss in setting the densities with $1/f$ noise generated by a 3 dimensional FFT. They make convincing clouds. Unfortunately, it is unlikely that this method will elicit realistic dynamical behavior.

A second set of models which appears promising is Reeves' particle systems (Reeves 1983). We can use his techniques to fill the density array by interpolation. Ray tracing can then be used to render the array. Flows of ODEs and PDEs can be used to model the action of flowing water and to model hair and fuzzy surfaces, as well as trees. These methods are obvious generalizations of Reeves' method.

Finally we mention actual physical models of the atmosphere to generate motion studies of clouds.

5.1 A Cloud Model for Generating Density Functions

A numerical model for cumulus convection is used to generate three-dimensional optical density functions. The model incorporates the equations of motion, continuity, condensation, and evaporation. It models the convective motions of the atmosphere, the latent heat of vaporization of water, and frictional effects. Coriolis effects due to the rotation of the Earth are ignored.

The cloud simulation commences in a convectively unstable atmosphere with high relative humidity. A constant heat source is applied at the base of the model, representing sunlight heating the earth. In the model, a warm layer of air forms close to the ground, and starts to rise. The cloud starts forming as soon as moist air rises enough to become supersaturated. The output of the model is the mixing ratio of liquid water in the atmosphere at each 3D grid point. The liquid water mixing ratio is directly interpreted as the optical density of the cloud. An image is then generated from these optical densities using the diffuse rendering algorithm.

The following symbols are used to represent atmospheric quantities:

u, v, w	wind velocities in the x, y , and z directions, respectively
V	the velocity vector consisting of the components (u, v, w)
F	the friction vector consisting of the components (F_x, F_y, F_z)
θ	potential temperature
q	total water mixing ratio
q_l	liquid water mixing ratio

Nine equations define the model. The first three equations define the acceleration of an air parcel. Acceleration is determined from the momentum of the airflow, frictional effects, and from buoyancy.

$$\begin{aligned}\frac{\partial u}{\partial t} &= -V \cdot \nabla u - F_x \\ \frac{\partial v}{\partial t} &= -V \cdot \nabla v - F_y \\ \frac{\partial w}{\partial t} &= -V \cdot \nabla w - F_z + \theta\end{aligned}$$

The buoyancy term is proportional to the potential temperature of the air parcel, θ . Potential temperature is defined as the temperature an air parcel would have if it were brought down to sea level. It is more convenient to use in the model instead of absolute temperature for the following reason: as an air parcel ascends, its temperature will decrease due to the decreasing pressure, and must be recalculated at each altitude

of the air parcel. However, the potential temperature of the air parcel will remain constant. Therefore, it is computationally more efficient to use potential temperature instead of absolute temperature in the model. Potential temperature effectively measures the amount of heat energy contained in an air parcel.

The change in potential temperature is determined by the advection of temperature into the local region and the heat released by condensing cloud vapor. The term "advection" is used to describe the change of a parameter at a fixed location due to transportation by the winds. Thus an increase in potential temperature due to transportation of warm air into the local region is called advective warming. An external heat source such as sunlight is represented by the variable Q :

$$\frac{\partial \theta}{\partial t} = -V \cdot \nabla \theta + \frac{L_{vw}}{c_p} \frac{\partial q_l}{\partial t} + Q.$$

L_{vw} is the latent heat of vaporization of water. c_p is the specific heat of air at constant pressure.

Frictional effects are approximated by a simple relation yielding an exponential decay of wind velocities with time:

$$F = \frac{1}{t_f} V$$

where t_f is the friction timescale.

The equation of continuity constrains the motions of the air parcels. The requirement is that air is neither created nor destroyed at any given location, which implies that

$$\nabla \cdot V = 0.$$

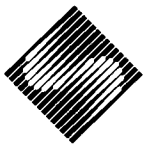
The density of air is assumed to be constant over the scale of the model. A corollary of this requirement is that the upward velocity over any horizontal plane in the model must average to zero.

The change in water mixing ratios is determined by the advection of water and the amount of evaporation and condensation which takes place. Evaporation is assumed to take place until the air is saturated or all the liquid water is evaporated. Condensation takes place whenever the air is supersaturated. The change in total water content is simply determined by the advection of water:

$$\frac{\partial q}{\partial t} = -V \cdot \nabla q$$

The saturation mixing ratio at any given level is an exponential function of altitude:

$$q_s = A \exp^{-\alpha z}$$



where A and α are exponential scaling constants. q_* is interpreted to be the mass ratio of water to air at saturation for a given volume of air. The constants are determined by the boundary conditions that $q_* = 0.02$ at the bottom level of the model, and $q_* = 0.002$ at the top of the model. The liquid water mixing ratio is determined by the amount of water present in the air parcel in excess of the saturation mixing ratio:

$$q_l = \max(q - q_*, 0).$$

An important advantage of using a physical model for clouds is that the cloud evolves realistically with time. This approach lends itself to realistic cloud animation whereas other modelling approaches do not automatically produce realistic cloud behavior. An animation of an evolving cumulus cloud is discussed in the next section.

§6 Computer Results

Figures 1 through 4 show the low albedo rendering technique with fractal volume densities. Figure 1 is defined on a $16 \times 16 \times 16$ grid, while 2 and 3 show a cloud fractally generated on a $128 \times 128 \times 16$ grid. These frames were computed at 512×512 resolution on an IBM4341 processor. CPU times ranged from 1 to 4 hours. Figure 4 shows a fractal cloud in combination with a fractally generated mountain at 256×256 resolution, on the same machine this frame consumed 6 hours of CPU time.

Figures 5 through 10 show a cumulus cloud at various stages of development. The optical densities were calculated using the above model on a VAX 11/780 using a three dimensional grid of (10 by 10 by 20) grid elements. A simple forward-differencing scheme was used to integrate the above differential equations in time. Each time step took around 10 cpu seconds to compute, representing roughly one second of cloud evolution. The cloud was allowed to evolve for several minutes to generate the images shown. Rendering was done on an IBM4341 at 512×512 resolution, with CPU times of 2 hours each.

§7 Summary

This paper has presented new methods for the synthesis of images which contain volume densities. We have found that single scattering is a poor approximation for clouds when more general viewing geometries are used. We have offered a new method for solving the scattering equations in an approximate manner suitable for computer graphics. We have also presented

equations which will model the dynamic behavior of clouds.

§8 References

- Anselone, P.M., and Gibbs, A.G., 1974: Convergence of the discrete ordinates method for the transport equation, *Constructive and Computational methods for differential and integral equations*, Springer Verlag Lecture notes in math 430.
- Appel, A., 1968: Some techniques for shading machine renderings of solids, 1968 SJCC, 37-45.
- Blinn, J.F., 1982: Light reflection functions for simulation of clouds and dusty surfaces. Proc. SIGGRAPH82. In *Comput. Gr.* 16,3, 21-29.
- Chandrasekhar, S., 1950: *Radiative Transfer*, Oxford University Press.
- Clark, T.L., 1979: Numerical Simulations with a three-dimensional cloud model: lateral boundary condition experiments and multicellular severe storm simulations. *J. of the Atmospheric Sciences*, 36, 2191.
- Courant, R. and Hilbert, D., 1953: *Methods of Mathematical Physics* v.1, Interscience, New York.
- Dahlquist, G., and Bjork, A., 1974: *Numerical Methods*, Prentice Hall, New York.
- Goldstein, E. and Nagle, R. 1971: 3D visual simulation, *Simulation* 16, 25-31.
- Kajiya, J.T., 1983: Ray tracing procedurally defined objects, SIGGRAPH83, *Comput. Gr.* 17,3, 91-102.
- Kajiya, J.T., 1982: Ray tracing parametric patches, SIGGRAPH82, *Comput. Gr.* 16,3, 245-254.
- Keller, H.B., 1960a: Approximate solutions of transport problems, *SIAM J. Appl. Math.* 8, 43-73.
- Keller, H.B., 1960b: On the pointwise convergence of the discrete ordinates method, *SIAM J. Appl. Math.* 8, 560-567.
- Max, N., 1983: Panel on the simulation of natural phenomena, Proc. SIGGRAPH83, In *Comput. Gr.* 17,3, 137-139.
- Schlesinger, R.E., 1975: A three-dimensional numerical model of an isolated deep convective cloud: Preliminary results. *J. of the Atmospheric Sciences*, 32, 934-957.
- Schlesinger, R.E., 1978: A three-dimensional numerical model of an isolated thunderstorm, part I: comparative experiments for variable ambient wind shear. *J. of the Atmospheric Sciences*, 35, 690-713.
- Schlesinger, R.E., 1980: A three-dimensional numerical model of an isolated thunderstorm, part II: dynamics

of updraft splitting and mesovortex couplet evolution. *J of the Atmospheric Sciences*, 37, 395.

Simpson, J., Van Helvoirt, G., McCumber, M., 1982: Three-dimensional simulations of cumulus congestus clouds on GATE day 261. *J. of the Atmospheric Sciences*, 39, 126.

Reeves, W.T., 1983: Particle systems—a technique for modeling a class of fuzzy objects, *ACM Trans. on Graphics*, 2,2.

Voss, R., 1983: Fourier synthesis of gaussian fractals: $1/f$ noises, landscapes, and flakes, *Tutorial on State of the Art Image Synthesis* v.10, SIGGRAPH83.

Wallace, J. M., and Hobbs, P. V., 1977: *Atmospheric Science*, Academic Press, pp.359-407.

Whitted, T., 1980: An improved illumination model for shaded display, *Comm. ACM* 23, 343-349.

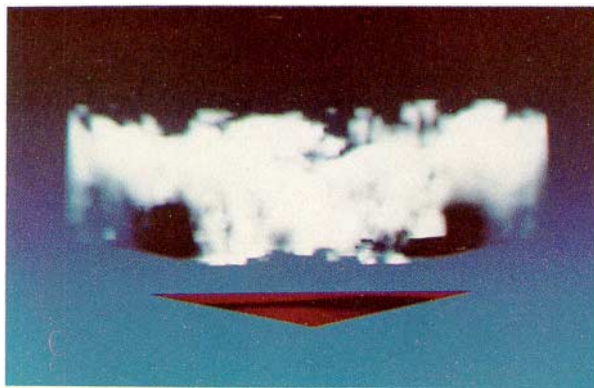


Fig. 3

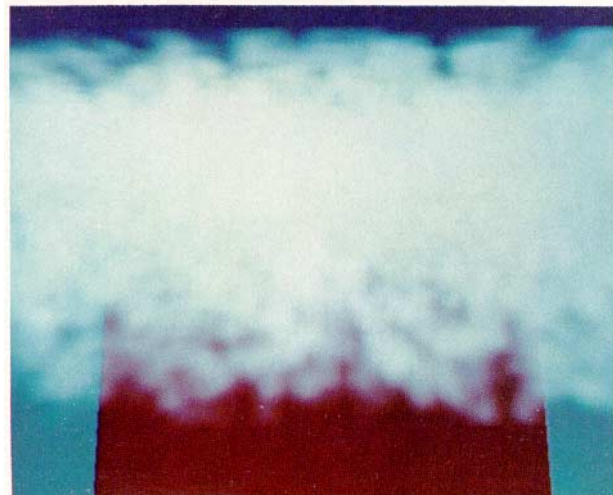
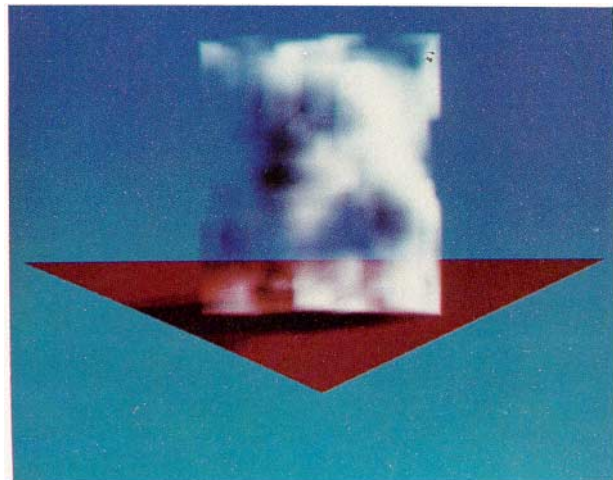


Fig. 1&2



Fig. 4

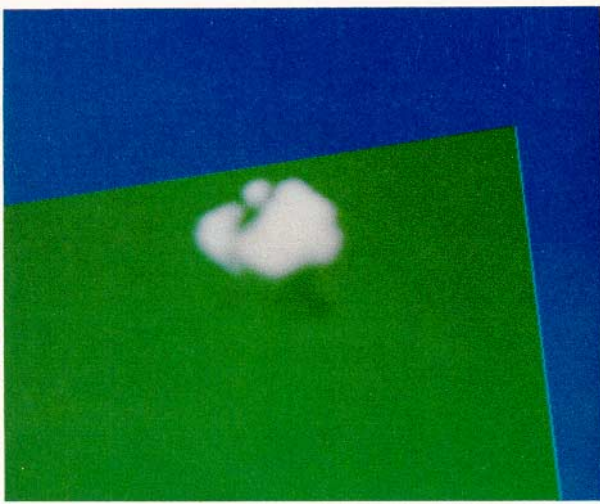
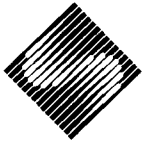


Fig. 5

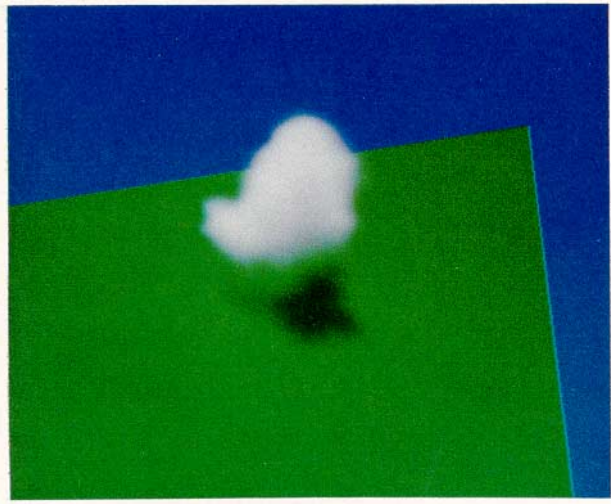


Fig. 8

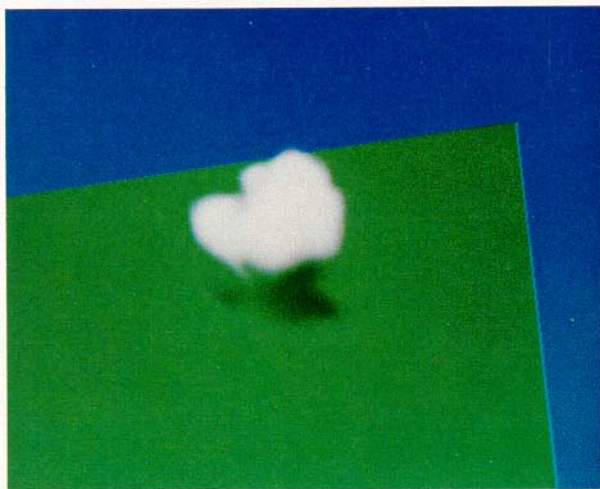


Fig. 6

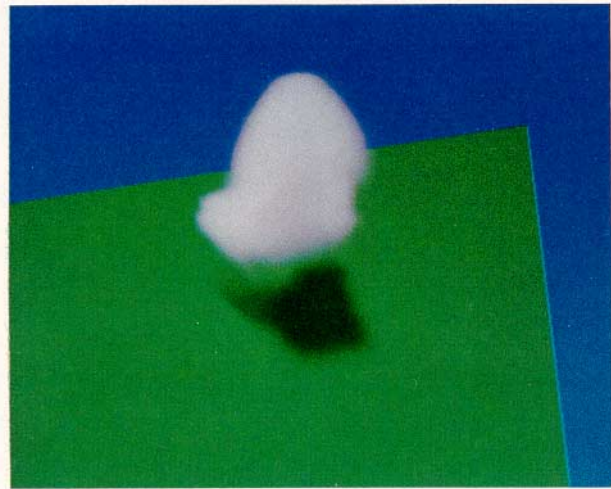


Fig. 9

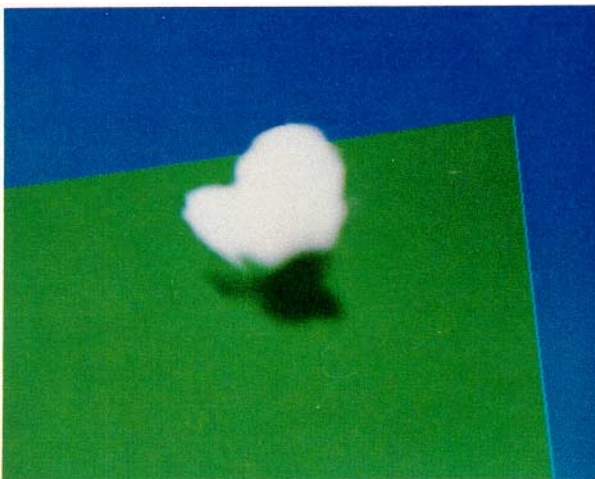


Fig. 7



Fig. 10